Cosserat shape effects in the bending of foams

R. S. Lakes*
Department of Engineering Physics and Department of Materials Science,
University of Wisconsin, Madison, WI 53706
* rlakes@wisc.edu

September 12, 2023

Preprint, R. S. Lakes, Cosserat shape effects in the bending of foams, Mechanics of Advanced Materials and Structures, Volume 30, Issue 19 Pages 3997-4001 (2023). https://doi.org/10.1080/15376494.2022.2086328

Abstract

In classical pure bending of a bar of square cross sections, two lateral surfaces undergo anticlastic curvature and the other two lateral surfaces undergo tilt. If the bar is made of a Cosserat solid, the tilted lateral surfaces deform in a sigmoid shape in addition to tilt. Parametric studies reveal the bulge depends on the bending characteristic length, the coupling number, and the ratio of two Cosserat rotation gradient constants. This sigmoid bulge deformation is observed in two foams and is found to be consistent with predictions using elastic constants obtained from size effect studies.

1 Introduction

Physical properties including elastic constants, dielectric permittivity, piezoelectric sensitivity and thermal expansion are customarily described using continuum concepts even though no physical material is actually a continuum; there is always microstructure. The classical continuum representation is warranted provided the structure size is sufficiently small compared with the size scale of the experiment or the application. The assumption of of negligible structure size comes into question if one considers nanoscale objects in comparison with interatomic distances or the size of physical objects in comparison with the size scale in composites and rib lattices. In such cases classical continuum representations may not be applicable. One may retain the utility and predictive power of continuum theory provided additional freedom is incorporated in the continuum analysis as is the case in generalized continuum theories.

Classical linear elasticity predicts the torsion and bending rigidity of rods to be proportional to the fourth power of the diameter. Deviations from this prediction are known as size effects. Size effects can be dealt with using generalized continuum theories such as Cosserat [1] [2] also called micropolar [3] elasticity, which incorporates local rotation of points as well as the translation. The isotropic Cosserat theory incorporates six elastic constants in contrast to classical in which there are two. Two of the constants can be expressed as characteristic lengths, explained below; one is a coupling number that quantifies the degree of coupling between local rotations and displacement gradient.

Size effects are well known in experiments on heterogeneous materials viewed as Cosserat solids. Specifically the rigidity of rods in torsion and bending differs from the predictions of classical

elasticity; slender rods are stiffer than anticipated based on classical theory as is predicted from analysis [4] and observed experimentally in foams [5] [6] [7], in plates with a periodic array of holes, [8], and in designed rib lattices [9]. Shape effects also occur. In torsion of a square cross section bar, the warp of cross sections is predicted to be reduced [11] [12] compared with classical analysis. Such warp reduction has been observed experimentally [13] [14] [15]. In bending of a square cross section bar, the surfaces that classically tilt under bending also undergo a sigmoid bulge deformation orthogonal to the surface (Figure 1) if the material is a Cosserat solid [16]. Here we illustrate detailed effects of the Cosserat elastic constants on the nonclassical deformation and present experimental results for the nonclassical bulge.

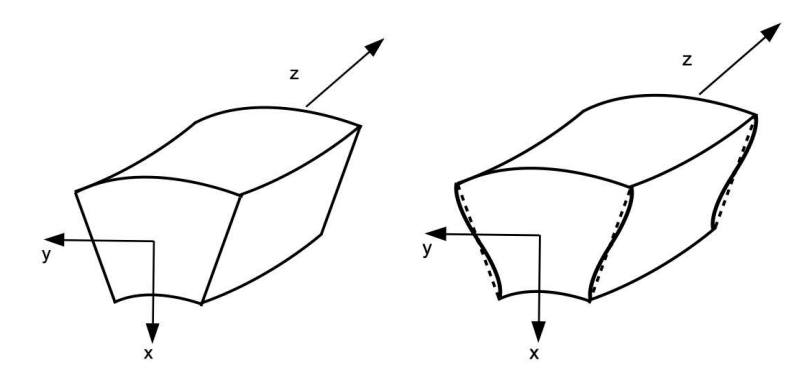


Figure 1: Bending of a square section bar. Left, classical; right, Cosserat sigmoid bulge.

2 Methods

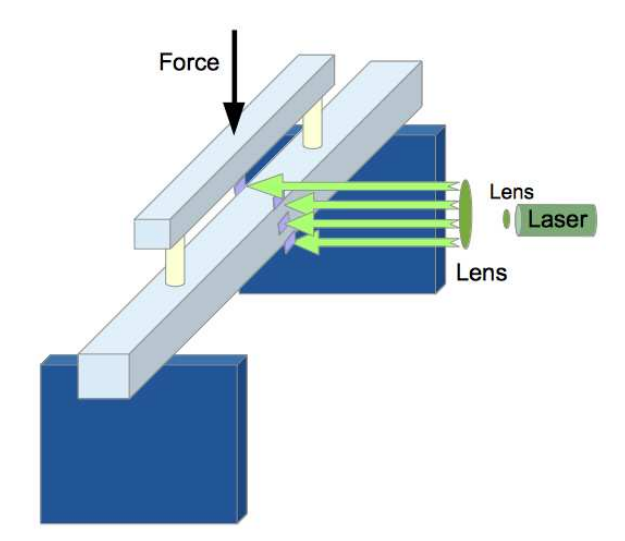


Figure 2: Setup for bending of a square section bar. Laser light was reflected from mirrors upon the bar to reveal rotations.

Materials studied are a low density open cell polyurethane foam and a relatively stiff dense polyurethane foam. Both foams were found to be isotropic in prior studies. The low density foam had a density of 30 kg/m^3 and an average pore size of 0.3 mm. Size effect studies [6] disclosed E

= 81 kPa, characteristic length in bending $\ell_b = 2.2$ mm, coupling number N = 0.99, $\frac{\beta}{\gamma} = 0.8$. The specimen used for the present study was 25 mm in square cross section.

The dense foam was closed cell; the density was 340 kg/m³ with a range of cell size from 0.05 to 0.15 mm. Size effect studies [7] disclosed E=300 MPa, $\ell_b=0.456$ mm, N=0.152, $\frac{\beta}{\gamma}=0.944$. The specimen used for the present study was 10.7 mm wide and 9.5 mm deep in cross section. Ψ was inferred but is not pertinent to bending. Elastic constants are defined in the following section.

Specimens were mounted on a vibration isolating optical table. The low density open cell foam was deformed by cementing the ends to optical tilt stages and applying a tilt motion to the ends via micrometer screws to achieve pure bending. The dense polyurethane foam was deformed in four point bending as shown in Figure 2 using dead weights below the optical table to apply a force via a hook upon the illustrated cross bar.

The slope of small deformed regions on the lateral surfaces was measured by reflecting a diverged and collimated laser beam from mirrors attached to the specimen and determining the angular motion of the reflected beams. For the dense foam, mirrors 6 mm square were placed on rubber offsets 3 mm in diameter (not shown). Mirrors were provided on the front and back surfaces of the bar as shown to determine overall rotation. The offsets at the edges covered 1.5 mm of the foam bar. For the compliant open cell foam, 3 mm square mirrors were cemented to the foam.

The angular displacement revealed by the optical method provides the slope of the lateral surface deformation curve. In comparison with point-wise measurements of displacement which contain scatter due to material heterogeneity, the rotation method provides some averaging. Reflected laser spots were projected on a calibrated screen on a wall, permitting positions to be recorded nearly simultaneously to eliminate effects of creep deformation. A constant corresponding to the tilt was subtracted to obtain the slope associated with sigmoid deformation for comparison with the classical slope associated with Poisson deformation. A slope that does not depend on position is a signature of classical elasticity. By contrast, in a Cosserat solid, slope varies with position in a characteristic way due to sigmoid bulge of the lateral surfaces.

3 Analysis

The isotropic Cosserat [1] equations are [3]

$$\sigma_{ij} = 2G\epsilon_{ij} + \lambda \epsilon_{kk} \delta_{ij} + \kappa e_{ijk} (r_k - \phi_k) \tag{1}$$

$$m_{ij} = \alpha \phi_{k,k} \delta_{ij} + \beta \phi_{i,j} + \gamma \phi_{j,i} \tag{2}$$

in which σ_{ij} is the force stress tensor, m_{ij} is the couple stress tensor (moment per unit area, asymmetric in general), $\epsilon_{ij} = (u_{i,j} + u_{j,i})/2$ is the small strain tensor, u_i the displacement vector, and e_{ijk} is the permutation symbol. The Cosserat microrotation vector ϕ_i in is kinematically distinct from the macrorotation vector $r_i = (e_{ijk}u_{k,j})/2$. ϕ_i refers to the rotation of points themselves, while r_i refers to the rotation associated with movement of nearby points. The usual Einstein summation convention for repeated indices is employed, and a comma denotes differentiation with respect to ensuing subscripts which represent spatial Cartesian coordinates. Cosserat solids are also called micropolar [3].

The six Cosserat elastic constants are λ , G, α , β , γ , and κ . G is the shear modulus and λ is the Lamé elastic constant with the same interpretation as in classical elasticity. The following constants also have the same interpretation as in classical elasticity. The values are observed in the absence of gradients. Young's modulus $E = \frac{(2G)(3\lambda + 2G)}{2\lambda + 2G}$, shear modulus G, Poisson's ratio $\nu = \frac{\lambda}{2(\lambda + G)}$. There are two independent isotropic elastic constants as a result of known interrelations.

Technical Cosserat constants are as follows: characteristic length, torsion $\ell_t = \sqrt{\frac{\beta + \gamma}{2G}}$, characteristic length, bending $\ell_b = \sqrt{\frac{\gamma}{4G}}$, coupling number $N = \sqrt{\frac{\kappa}{2G + \kappa}}$, polar ratio $\Psi = \frac{\beta + \gamma}{\alpha + \beta + \gamma}$.

Cosserat elastic constants may be determined as follows. Moduli E and G are revealed by tension and shear tests in the absence of gradients or by bending and torsion of sufficiently large specimens to achieve asymptotic behavior. The torsion characteristic length ℓ_t is revealed by size effect measurements in torsion for specimens that are relatively large in comparison with ℓ_t . The bending characteristic length ℓ_t is revealed by size effect measurements in bending for specimens that are relatively large in comparison with ℓ_t . The coupling number N and polar ratio Ψ are obtained from size effect measurements for sufficiently slender specimens. One may also determine N by determining ℓ_t from size effect studies in torsion, then obtaining N from measurements of warp in torsion of a bar of square cross section.

Cosserat effects may also be probed by study of nonclassical fields of deformation. For example in torsion of square cross section bars, the warp is reduced [12] in comparison with classical predictions. In bending, the transverse surfaces that tilt in a classical solid also undergo a sigmoid deformation in a Cosserat solid.

The classical three-dimensional displacement field solution for pure bending of prismatic bars in isotropic linear elasticity is

$$u_x = -\frac{z^2 + \nu(x^2 - y^2)}{2R}, \quad u_y = -\nu \frac{xy}{R}, \quad u_z = \frac{xz}{R},$$
 (3)

in which R is the principal radius of curvature of bending. Referring to Figure 1 the bending is produced by pure moments about the y-axis. If the material is a Cosserat solid [16], the classical displacement field provides a solution provided $\beta/\gamma = -\nu$. For that case, there are size effects in the bending rigidity because couple stresses contribute to the moment M. In the following, E is Young's modulus, a is the bar half width and I is the area moment of inertia.

$$M = \frac{EI}{R} [1 + 24(\frac{\ell_b}{2a})^2 (1 - \nu)] \tag{4}$$

which gives a rigidity ratio (observed rigidity divided by classical rigidity)

$$\Omega = [1 + 24(\frac{\ell_b}{2a})^2(1-\nu)]. \tag{5}$$

If $\beta/\gamma \neq -\nu$, then additional terms [10] appear in the size effect expression [16].

We compare these size effects with those of Gauthier [4] for plate bending. Size effects in cylindrical bending of a plate of thickness h are given by a rigidity ratio $\Omega = [1 + 12(\frac{d}{h})^2]$, with $d = \frac{\gamma}{E}(1 - \nu^2)$. Because we define $\ell_b = \sqrt{\frac{\gamma}{4G}}$, and with the isotropic interrelation $E = 2G(1 + \nu)$, then $d = 2\frac{\ell_b}{h}(1 - \nu)$. So the Ω given in [4] corresponds to Eq. (5). The plate deformation for a general set of elastic constants requires moments on all four edge surfaces, but if $\beta/\gamma = -\nu$, then moments on two surfaces will suffice, consistent with our assumptions for the square cross section beam.

The solution [16] for bending of the square Cosserat elastic bar is rather complicated. If the Poisson's ratio $\nu=0.3$, corresponding to the materials under study, there is considerable simplification. The lateral bulge depends on the elastic constants, assuming $\nu=0.3$, as follows. The Cosserat solution for u_y contains contributions to tilt in addition to the Poisson effect in Eq. (3); these are omitted here to reveal the sigmoid bulge.

The sigmoid bulge at the surface y = a is given by

$$u_y = b_2 \left(\frac{x^3}{a} - xa\right). (6)$$

The slope, after subtracting a constant term to compare the bulge effect with the classical slope $du_u/dx|_{cl} = -\nu\epsilon$ is

$$\frac{du_y}{dx} = -0.3 + b_2 \left(3x^2/a - a \right) \tag{7}$$

in which

$$b_2 = -\frac{28}{3}a_3 \tag{8}$$

$$a_1 = \frac{d}{250} \left(730N^4 + (\frac{\ell_b}{a})^2 N^2 \left(19370 - 55209N^2 \right) + 36(\frac{\ell_b}{a})^4 \left(3115 - 49871N^2 - 5649N^4 \right) \right)$$
(9)

$$a_3 = \frac{7}{6} \left(\left((30a_1 + 13a_4) \left((\frac{\ell_b}{a})^{-2} \frac{1}{18} + \frac{1}{N^2} - 1 \right) \right) - 3a_4 \right) \left(30 + 19 \left(\frac{1}{N^2} + (\frac{\ell_b}{a})^{-2} \frac{1}{18} \right) \right)^{-1}$$

$$(10)$$

$$a_4 = -\frac{21}{100}d\left(49N^4 + 2\left(\frac{\ell_b}{a}\right)^2N^2\left(841 - 798N^2\right) + 36\left(\frac{\ell_b}{a}\right)^4\left(400 - 1541N^2 - 168N^4\right)\right)$$
(11)

$$d = \frac{75((\frac{\ell_b}{a})^2 N^2 (3+10\frac{\beta}{\gamma}))}{2R} / \left[1630N^6 + 108((\frac{\ell_b}{a})^6 (28525+93980N^2+42889N^4+1176N^6)) + 3((\frac{\ell_b}{a})^4 N^2 (497150+625965N^2+60501N^4) + 210((\frac{\ell_b}{a})^2 N^4 (489+205N^2)) \right].$$
(12)

Sigmoid bulge varies with coupling number N as shown in Figure 3 for $\ell_b/a=0.2$, in Figure 4 for $\ell_b/a=0.1$ and in Figure 5 for $\ell_b/a=0.05$. The bulge is normalized such that $U=u_y/\epsilon a$. If $\ell_b<0.2$, the bulge increases monotonically with N but for $\ell_b>0.2$, bulge increases with N up to 0.6, then decreases.

If the characteristic length is small in comparison to the bar half width, then the effect of N is reduced as shown in Figure 4 and Figure 5. If $\ell_b << a$ the effects are small but they are comparatively insensitive to N as shown in Figure 6. A similar effect is known in size effects; in larger specimens, the gradients are smaller, so the driving force for the micro and macro rotations to be unequal are smaller.

The direction of bulge depends on β/γ as shown in Figure 7. If $\beta/\gamma = -\nu$, then the deformation field is identical with the classical field. Size effects occur but not shape effects; there is no sigmoid bulge in this case. For β/γ sufficiently negative, the direction of the sigmoid bulge will reverse.

The effect of N was also examined in the vicinity of the limit $\beta/\gamma = -\nu$. Bulge effects were small in this region but were nonetheless monotonically increasing with N, similarly to the behavior for large β/γ .

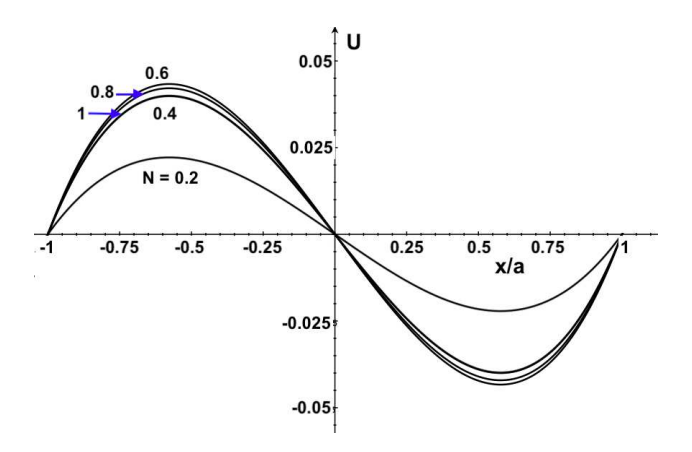


Figure 3: Sigmoid bulge U vs. position x/a for $N=0.2,\,0.4,\,0.6,\,0.8,\,1;\,\ell_b/a=0.2,\,\beta/\gamma=0.95.$

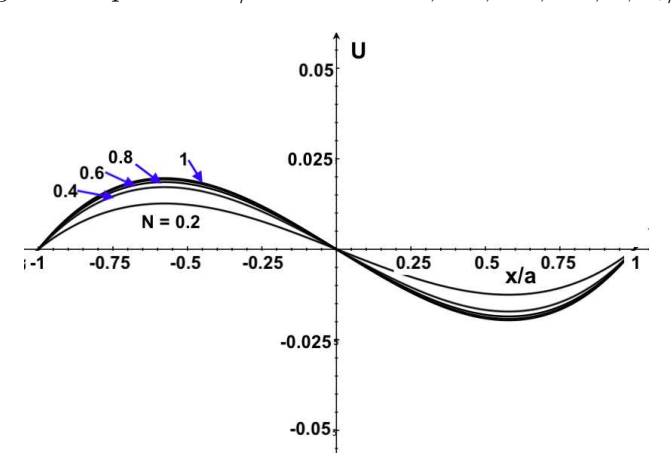


Figure 4: Sigmoid bulge U vs. position x/a for $N=0.2,\,0.4,\,0.6,\,0.8,\,1;\,\ell_b/a=0.1,\,\beta/\gamma=0.95.$

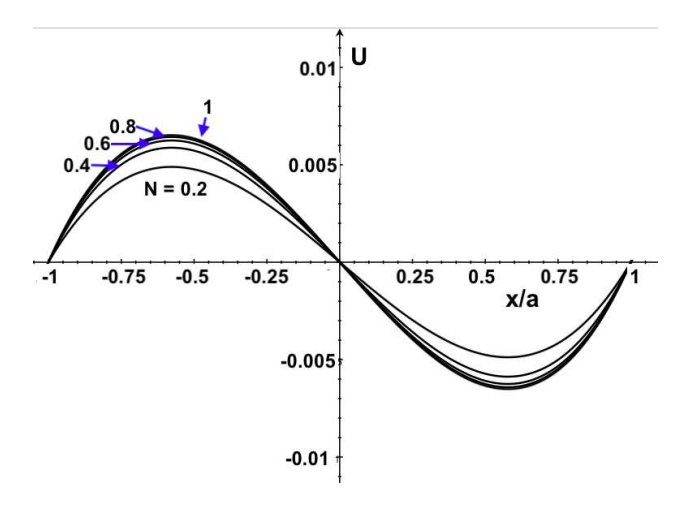


Figure 5: Sigmoid bulge U vs. position x/a for $N=0.2,\,0.4,\,0.6,\,0.8,\,1;\,\ell_b/a=0.05,\,\beta/\gamma=0.95.$

4 Experimental Results

Experimental results for angular displacement or slope are compared with theoretical predictions based on size effects in the following. Following [16], the bar width is 2a. Figure 8 shows the

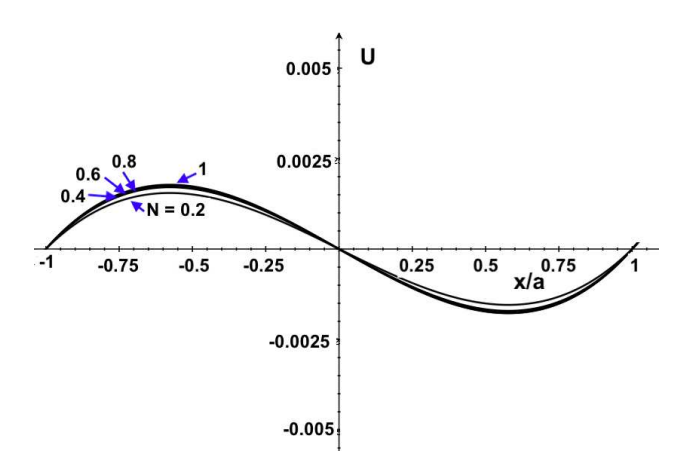


Figure 6: Sigmoid bulge U vs. position x/a for $N = 0.2, 0.4, 0.6, 0.8, 1; <math>\ell_b/a = 0.025, \beta/\gamma = 0.95$.

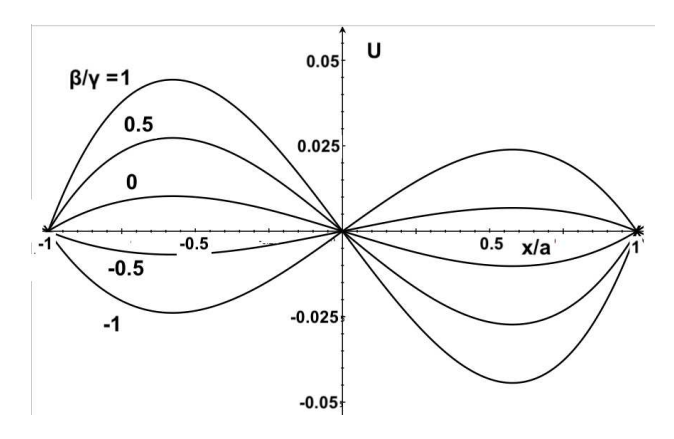


Figure 7: Sigmoid bulge U vs. position x/a for $N=0.5, \ell_b/a=0.2, \beta/\gamma=-1, -0.5, 0, 0.5, 1.$

comparison of predicted and observed magnitude of slope S (normalized to strain as with U) for a low density open cell foam. Sigmoid bulge effects were pronounced as anticipated based on the large coupling number N and the relatively large characteristic length ℓ_b in comparison with the specimen width. For a classical elastic material, there is no bulge, only a tilt, corresponding to a slope S that is constant with position.

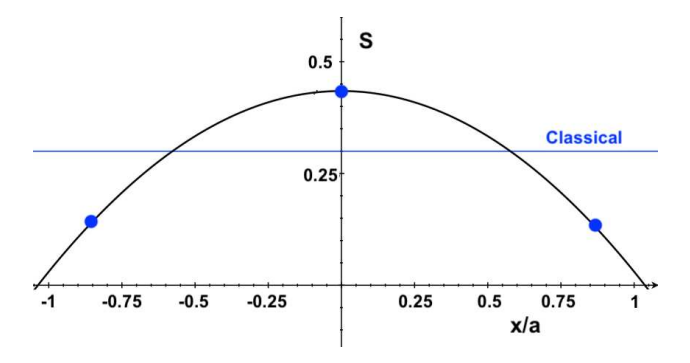


Figure 8: Slope S vs. position x/a for $N=0.99, \ell_b/a=0.18, \beta/\gamma=0.8$; points, experiment for low density foam. The horizontal line is the classical slope.

Figure 9 shows the comparison for a dense closed cell foam. Observed sigmoid bulge effects were considerably smaller in this material than in open cell foam. The coupling number N obtained from size effects was small at 0.15, giving rise to smaller predicted effects than for the open cell foam.

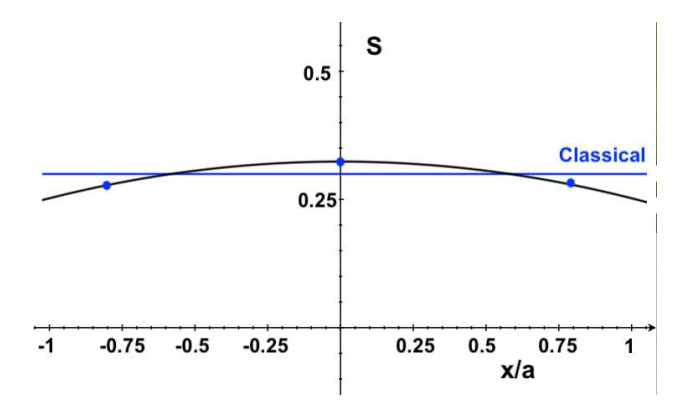


Figure 9: Slope S vs. position x/a for N = 0.15, $\ell_b/a = 0.115$ $\beta/\gamma = 0.94$; points, experiment for dense foam. The horizontal line is the classical slope.

The comparisons show consistency of observations with predictions from size effects. Such comparisons are not unique because the sigmoid bulge increases with ℓ_b , N and $\beta/\gamma+\nu$. Observation of sigmoid bulge effects in a single bending experiment suffices to demonstrate nonclassical effects but not to determine the elastic constants. As with the method of size effects, multiple experiments would be needed to determine the elastic constants.

5 Discussion

Sigmoid curvature of the lateral surfaces reveals Cosserat effects, the magnitude of which depends on $\beta/\gamma + \nu$, ℓ_b , and N. For normal Poisson's ratio, a reversal of the curvature is predicted to occur if β/γ is sufficiently negative. One may also extract β/γ from a comparison of size effects in bending and torsion. Sigmoid bulge increases with ℓ_b and with $\beta/\gamma + \nu$. A monotonic increase of bulge with coupling number N is predicted if ℓ_b is not too large compared with the bar width. A single measurement of sigmoid bulge of the lateral surfaces in bending suffices to demonstrate nonclassical behavior but the bulge depends on a combination of elastic constants. Measurement of bulge combined with size effect measurements can reveal the coupling number N even in cases for which the set of elastic constants renders it difficult to extract from size effect measurements alone.

Cosserat elasticity suffices to interpret the present experiments. Observed tilt variations associated with bulge are consistent with Cosserat elastic constants obtained from prior size effect measurements.

Cosserat elasticity is not the only generalized continuum theory. The Mindlin microstructure theory [17], also called micromorphic elasticity, allows the local rotation as well as the local strain to differ from the macroscopic rotation and strain. This theory is more general than Cosserat elasticity and admits 18 elastic constants for an isotropic material. The theory of elastic materials with voids [18] is a different subset of microstructure theory that allows the solid to be sensitive to gradients in dilatation but not in rotation. It predicts size effects in bending but not in torsion so it cannot represent the present foams or in lattices previously studied. Micromorphic freedom could occur; the present interpretation deals only with Cosserat freedom and the comparison with classical elasticity.

6 Acknowledgment

We gratefully acknowledge support by the National Science Foundation via Grant No. CMMI -1906890.

References

- [1] E. Cosserat and F. Cosserat, Theorie des Corps Deformables, Hermann et Fils, Paris (1909).
- [2] R. D. Mindlin, Stress functions for a Cosserat continuum, Int. J. Solids Structures, 1, 265-271 (1965).
- [3] A. C. Eringen, Theory of micropolar elasticity. In Fracture Vol. 1, 621-729 (edited by H. Liebowitz), Academic Press, New York (1968).
- [4] R. D. Gauthier and W. E. Jahsman, A quest for micropolar elastic constants. J. Applied Mechanics, 42, 369-374 (1975).
- [5] R. S. Lakes, Experimental microelasticity of two porous solids, International Journal of Solids and Structures, 22 55-63 (1986).
- [6] Z. Rueger and R. S. Lakes, Experimental Cosserat elasticity in open cell polymer foam, Philosophical Magazine, 96 (2), 93-111, (2016).
- [7] Z. Rueger and R. S. Lakes, Experimental study of elastic constants of a dense foam with weak Cosserat coupling, Journal of Elasticity 137(1), 101-115, (2019).
- [8] A. J. Beveridge, M. A. Wheel and D. H. Nash, The Micropolar Elastic Behaviour of Model Macroscopically Heterogeneous Materials, International Journal of Solids and Structures, 50, 246-255 (2013)
- [9] Z. Rueger and R. S. Lakes, Strong Cosserat elasticity in a transversely isotropic polymer lattice, Physical Review Letters, 120, 065501 Feb. (2018).
- Z. Rueger, C. S. Ha and R. S. Lakes, Cosserat elastic lattices, Meccanica, 54(13), 1983-1999, (2019).
- [11] H. C. Park and R. S. Lakes. Torsion of a micropolar elastic prism of square cross section, Int. J. Solids, Structures, 23, 485-503 (1987).
- [12] W. J. Drugan and R. S. Lakes., Torsion of a Cosserat Elastic Bar with Square Cross-Section: Theory and Experiment, Zeitschrift fur angewandte Mathematik und Physik (ZAMP), 69(2), 24 pages (2018).
- [13] R. S. Lakes, D. Gorman, and W. Bonfield, Holographic screening method for microelastic solids, J. Materials Science, 20 2882-2888 (1985).
- [14] W. B. Anderson, R. S. Lakes, and M. C. Smith, Holographic evaluation of warp in the torsion of a bar of cellular solid, Cellular Polymers, 14, 1-13, (1995).
- [15] R. S. Lakes, Reduced warp in torsion of reticulated foam due to Cosserat elasticity: experiment, Zeitschrift fuer Angewandte Mathematik und Physik (ZAMP), 67(3), 1-6 (2016).
- [16] R. S. Lakes and W. J. Drugan, Bending of a Cosserat elastic bar of square cross section theory and experiment, Journal of Applied Mechanics, 82(9), 091002 (2015).
- [17] R. D. Mindlin, Micro-structure in linear elasticity, Arch. Rational Mech. Analy, 16, 51-78, (1964).
- [18] S. C. Cowin and J. W. Nunziato, Linear elastic materials with voids, J. Elasticity 13 125-147 (1983).